Paper 60

©Civil-Comp Press, 2012
Proceedings of the Eighth International Conference
on Engineering Computational Technology,
B.H.V. Topping, (Editor),
Civil-Comp Press, Stirlingshire, Scotland

Numerical Methods for Digitally Synthetic Holograms

A. Lotfi
Séchenyi István University
Győr, Hungary

Abstract

The main purpose of this paper is to develop a program package which generates artificial holograms by numerical methods and these computer generated holograms are numerically reconstructed. For the calculation of light propagation needed in the generation of holograms or in the reconstruction of the object from the hologram, two strategies are used. The first is the Fourier-based algorithm where the diffraction integral is approximated as a convolution integral, allowing computation using the fast Fourier transform algorithm. The second uses finite difference discretization to solve the parabolic wave equation. Numerical tests that assess the accuracy of these algorithms are presented.

Keywords: holography, computer generated hologram, Helmholtz equation, paraxial propagation, Fourier-based algorithm, finite difference method.

1 Introduction

Holography is one of the three-dimensional viewing techniques and uses the physical phenomena of interference and diffraction of light waves to record on a recording medium and to reconstruct a three-dimensional image. It is a two-step process: recording process and reconstruction process.
The first is the registration of the hologram of an object with the aid of CCD camera or photographic medium realized on the laboratory stand. The second is to obtain the holographic image of the original object registered by the recording medium [2] [4].
The development of computer technology allows us to transfer both the recording process and the construction process into the computer. The main purpose of this article is to develop a program package which generates artificial holograms by numerical methods and these computer generated holograms are numerically reconstructed. The fundamental problem in computational holography is the computation of the optical light field distribution which arises over the entire 3D

space. The result of this computation is used to reconstruct the original object at the image plane and the computation techniques used affect the quality of the reconstructed images.
The most commonly used numerical method to solve the scalar wave equation is the Fourier-based method developed by J.W. Goodman [1]. This approach is attractive since it requires little programming effort. The evaluation of the solution can be done by a FFT at each spatial position for which the field distribution is desired. Alternatively, we propose an algorithm to solve the problem directly in the time domain, which, consists of the discretization of the differential operator in scalar wave equation, such as the Finite-Difference Method (FDM).
In this paper we present two different beam propagation methods to simulate the propagation of the light field under the paraxial condition, the first is based on the fast Fourier transformation (FFT-BPM) [8] and the second based on the Finite-Difference Method (FD-BPM) [10]. The beam propagation method (FFT-BPM) proved to be an efficient tool for solving this type of problems. However, in application of this method to problems with very large cross-section one has to cope with the increased storage and reduced efficiency. The second numerical method to solve the wave equation is to use a finite difference approximation [12], based on the Peaceman-Rachford scheme. Following the finite-difference method (FDM) the wave equation is replaced by a system of linear equations. The resulting three-diagonal systems of equations are solved by some direct and iterative procedures [14].

This paper is organized as follows: In Section 2 we give a brief introduction to computational holography. In Section 3 we introduce the solution of the diffraction problem as Fresnel-Kirchhoff integral and we develop the numerical method to compute this integral. In Section 4 we introduce the parabolic wave equation and a finite-difference scheme to solve this equation on a three-dimensional grid. In Section 5 we present the results of numerical simulations using FFT-BPM and FD-BPM algorithm.

2 Method

Computational holography is the use of digital representations and computational methods to carry out holographic operations, modeling the physical phenomena of light diffraction in three-dimensional space and interference. The process of synthesizing a hologram generally consists of two steps: (1) the creation of the hologram and (2) the reconstruction of the hologram. In this work, either of these steps will be carried out numerically.

2.1 Mathematical Representation of the recording process

In the recording process, there are two basic waves that come together to create the interference pattern. All wavefronts are assumed to be mutually coherent sources of monochromatic light. The object wave front is represented by $\widetilde{O}$, which is the light

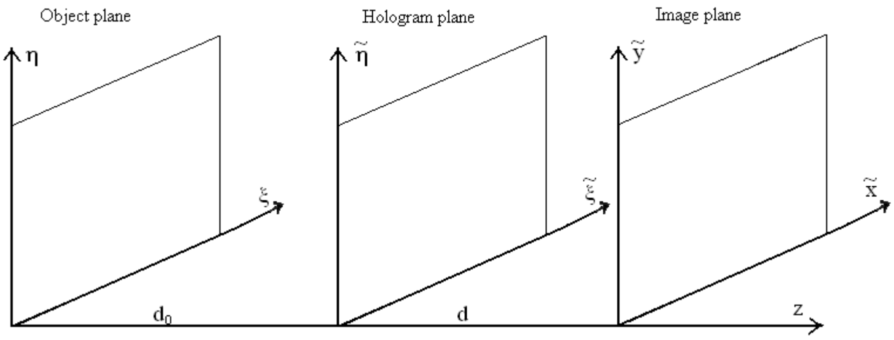

Figure 1: Coordinate system.

scattered from the object or light emitted by the object in object plane (ξ,η) (fig.1.) and propagated to the plane of the hologram $(\tilde{\xi},\tilde{\eta})$. Using the Fresnel-Kirchhoff integral, the object wavefront is calculated at the hologram plane and can be writing in the following form [4] [5]:

$$\tilde{O}(\tilde{\xi},\tilde{\eta}) = A_{\tilde{O}}(\tilde{\xi},\tilde{\eta})\exp\left[i\varphi_{\tilde{O}}(\tilde{\xi},\tilde{\eta})\right], \tag{1}$$

where $A_{\tilde{O}}$ and $\varphi_{\tilde{O}}$ are the real amplitude and the phase of the object beam.

Now suppose that the reference wave $\tilde{R}$ is incident on the $(\tilde{\xi},\tilde{\eta})$ plane. It can be similarly defined as:

$$\tilde{R}(\tilde{\xi},\tilde{\eta}) = A_{\tilde{R}}(\tilde{\xi},\tilde{\eta})\exp\left[i\varphi_{\tilde{R}}(\tilde{\xi},\tilde{\eta})\right], \tag{2}$$

where $A_{\tilde{R}}$ and $\varphi_{\tilde{R}}$ are the real amplitude and the phase of the reference beam.

These two wavefronts will interfere at the $(\tilde{\xi},\tilde{\eta})$ plane and produce a wave pattern. The total interference fringe intensity is $I_{\tilde{O}+\tilde{R}}$:

$$\begin{aligned} I_{\tilde{O}+\tilde{R}}(\tilde{\xi},\tilde{\eta}) &= \left|\tilde{O}(\tilde{\xi},\tilde{\eta}) + \tilde{R}(\tilde{\xi},\tilde{\eta})\right|^2 = \\ &= \left|\tilde{O}(\tilde{\xi},\tilde{\eta})\right|^2 + \left|\tilde{R}(\tilde{\xi},\tilde{\eta})\right|^2 + \tilde{O}(\tilde{\xi},\tilde{\eta})\tilde{R}^*(\tilde{\xi},\tilde{\eta}) + \tilde{O}^*(\tilde{\xi},\tilde{\eta})\tilde{R}(\tilde{\xi},\tilde{\eta}), \end{aligned} \tag{3}$$

where * represents complex conjugate. The term $\left|\tilde{O}(\tilde{\xi},\tilde{\eta})\right|^2$ is called object selfinterference and term $\left|\tilde{R}(\tilde{\xi},\tilde{\eta})\right|^2$ is called the reference bias. The terms $\tilde{O}(\tilde{\xi},\tilde{\eta})\tilde{R}^*(\tilde{\xi},\tilde{\eta})$ and $\tilde{O}^*(\tilde{\xi},\tilde{\eta})\tilde{R}(\tilde{\xi},\tilde{\eta})$ are the interference between the object wavefront and the reference beam.

2.2 Reconstruction process

The image reconstruction occurs when the hologram is illuminated by the same reference wave as the wave used in the recording process [6] [7]. In this case the image is reconstructed at the same distance from the hologram plane. The Fresnel-Kirchhoff formula can be applied for the image reconstruction. To obtain the transmission function, $\tilde{\Psi}(\tilde{\xi},\tilde{\eta})$, we have to multiply the complex amplitude of the hologram by the reconstruction reference wave:

$$\tilde{\Psi}(\tilde{\xi},\tilde{\eta}) = \tilde{R}(\tilde{\xi},\tilde{\eta}) I_{\tilde{O}+\tilde{R}}\left(\tilde{\xi},\tilde{\eta}\right) = \tilde{R}\left|\tilde{O}\right|^2 + \tilde{R}\left|\tilde{R}\right|^2 + \tilde{R}\tilde{O}\tilde{R}^* + \tilde{R}\tilde{O}^*\tilde{R}. \qquad (4)$$

The first and the second terms represent the zero diffraction order, the third and the fourth terms produce the virtual image and the real image [6]. The reconstruction leads to for different terms, whereas we are only interested in the real image and virtual image. To suppress the zero-order of the reconstruction wave front, we can use the so-called subtraction-mean-value method. The mean value over the whole hologram can be approximated by $I = \left|\tilde{O}\right|^2 + \left|\tilde{R}\right|^2$. In the reconstruction process, the first two terms can be suppressed by replacing $I_{\tilde{O}+\tilde{R}}$ with $(I_{\tilde{O}+\tilde{R}} - I)$ in Eq (4).

3 Description of diffraction

The light propagations described by the wave equation, which follows from Maxwell equations. The wave equation in vacuum is:

$$\Delta U(x,y,z,t) - \frac{1}{c^2}\frac{\partial^2 U(x,y,z,t)}{\partial^2 t} = 0 \qquad (5)$$

where c is the free space velocity of light, and Δ denotes the Laplace operator.
Assuming time-harmonic solutions $U(x,y,z,t) = U(x,y,z)e^{-j\omega t}$ (here, $U(x,y,z)$ is complex), in a homogeneous medium, U satisfies the scalar wave equation in the frequency domain [1] (Helmholtz, 1860):

$$\Delta U(x,y,z) + k^2 n^2(x,y,z) U(x,y,z) = 0 \qquad (6)$$

where $k = \omega / c = 2\pi / \lambda$ is the wavenumber in free space, λ is the wavelenght and n is the complex refractive index.

In this work we present two different beam propagation methods to simulate the propagation of the light field under the paraxial condition, the first is based on the fast Fourier transformation (FFT-BPM) [8] and the second based on the Finite-Difference Method (FD-BPM) [10].

3.1 The Beam Propagation Method (Fourier-based Algorithm)

The well known method used to obtain U in terms of its known value on some boundary is the Green's function method [1], which, function leads to the well known Kirchhoff diffraction integral solution.

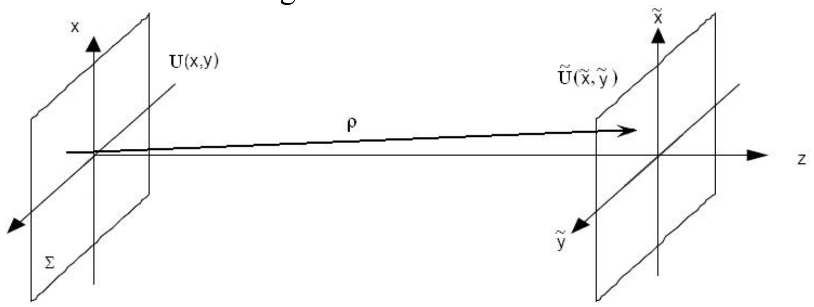

Figure 2: Coordinate system.

We assume that the initial field $U(x, y)$ is given on a plane (x, y) parallel to the observation plane $(\tilde{x}, \tilde{y})$ and located at z = 0 and z represents the direction of light propagation fig 2. Fresnel-Kirchhoff integral is used to compute the diffracted field on a plane $(\tilde{x}, \tilde{y})$ parallel to (x, y) at a distance d [1] [4] [5]:

$$\tilde{U}(\tilde{x}, \tilde{y}, d) = \frac{i}{\lambda} \iint_{\Sigma} U(x, y) \frac{\exp(-ik\rho)}{\rho} dxdy \tag{7}$$

where Σ is the area of the aperture, ρ is the distance between a point in the source plane and a point in the observation plane, λ is the light wavelength and $k = 2\pi / \lambda$ is the wave number. In Fresnel's approximation, the expression for ρ is approximated using the assumption that $d >> x, y, \tilde{x}, \tilde{y}$, i.e., that the distance to the observation plane is large compared to the size of the aperture and the image plane. In the denominator, the approximation $\rho \approx d$ is sufficient. In the exponent, we use the Taylor expansion $\sqrt{1+s} = 1 - s/2 + 3s^2/8 - ......$ for $|s| < 1$, to approximate ρ:

$$\rho = \sqrt{(\tilde{x}-x)^2 + (\tilde{y}-y)^2 + d^2} = d\sqrt{1 + \frac{(\tilde{x}-x)^2 + (\tilde{y}-y)^2}{d^2}} \approx d + \frac{(\tilde{x}-x)^2 + (\tilde{y}-y)^2}{2d} + ... \tag{8}$$

If the first two terms of the expansion are used. Inserting the above relation into the diffraction integral, Eq. (1) can be written in the form:

$$\tilde{U}(\tilde{x}, \tilde{y}, d) \approx \frac{i}{\lambda d} \exp(-ikd) \iint U(x, y) \exp\left[-i \frac{k}{2d} \left((\tilde{x}-x)^2 + (\tilde{y}-y)^2 \right) \right] dxdy \tag{9}$$

Evaluating the squares in the exponent, and moving the parts that are independent of x and y outside the integral yields the Fresnel diffraction integral:

$$
\begin{aligned}
\widetilde{U}(\widetilde{x},\widetilde{y},d) \approx \frac{i}{\lambda d}\exp(-ikd)\exp\left[-i\frac{k}{2d}\left(\widetilde{x}^2+\widetilde{y}^2\right)\right]\times \\
\times\iint\left\{U(x,y)\exp\left[-i\frac{k}{2d}\left(x^2+y^2\right)\right]\right\}\exp\left[i2\pi\left(\frac{\widetilde{x}}{\lambda d}x+\frac{\widetilde{y}}{\lambda d}y\right)\right]dxdy
\end{aligned}
\tag{10}
$$

The function $\widetilde{U}(\widetilde{x},\widetilde{y})$ can be digitized if the transmission function $U(x,y)$ is sampled on a rectangular raster of $N_x \times N_y$ matrix points, with step Δx and Δy along the coordinates. Then the discrete representation of Eq. (3) is given by the following formula [3]:

$$
\begin{aligned}
\widetilde{U}_d(m,n) \approx \frac{i}{\lambda d}\exp\left(-i\frac{2\pi}{\lambda}d\right)\exp\left[-i\pi\lambda d\left(\frac{m^2}{N_x^2\Delta x^2}+\frac{n^2}{N_y^2\Delta y^2}\right]\times \\
\sum_{k=0}^{N_x-1}\sum_{l=0}^{N_y-1}U(k,l)\exp\left[-i\frac{\pi}{\lambda d}\left(k^2\Delta x^2+l^2\Delta y^2\right)\right]\exp\left[i2\pi\left(\frac{mk}{N_x}+\frac{nl}{N_y}\right)\right]
\end{aligned}
\tag{11}
$$

where $m = 0.1....N_x - 1, \quad n = 0.1....N_y - 1$.

In observation plane, the image pixel dimensions $\Delta\widetilde{x}$ and $\Delta\widetilde{y}$ are related to the pixel dimensions Δx and Δy by:

$$\Delta\widetilde{x} = \frac{\lambda d}{N_x \Delta x} \text{ and } \Delta\widetilde{y} = \frac{\lambda d}{N_y \Delta y}.$$

In order to obtain high resolution in reconstructed image, a zero-padding method as suggested in [6] can be used by simple padding of the input data with zeros in both the horizontal and vertical directions. Now it is possible to evaluate the intensity and phase of the optical field by:

$$I(m,n) = \left|\widetilde{U}(m,n)\right|^2 = \left(\Re e\left[\widetilde{U}(m,n)\right]\right)^2 + \left(\Im m\left[\widetilde{U}(m,n)\right]\right)^2 \text{ and}$$

$$\phi(m,n) = \arctan\left(\frac{\Im m\left[\widetilde{U}(m,n)\right]}{\Re e\left[\widetilde{U}(m,n)\right]}\right).$$

In these equations $\Re e$ and $\Im m$ stand for the real and imaginary part of a complex field, respectively.

This approximation allows the calculation of the diffraction integral using a single Fourier transform. The whole process requires only Fourier transform, which is carried out using the FFT algorithm.

The aim of this work is to develop a program package which will be able to run on a one processor machine. Performing digital holographic operations such as FFT, on such large data sets requires high performance computing. Due to the extremely large transform size, implementation of the two-dimensional FFT is separated into one-dimensional FFTs, first applied over the rows and then over the columns [9] [10]. For a matrix stored in disk in row-major order that is too large to fit in memory, reading or writing a row will not cause performance problems, but the access pattern of reading or writing columns will significantly degrade performance. The most effective mechanism is to transpose the matrix between the one-dimensional FFTs. For computing the Fourier transform, we make use of the FFTW library [12] a freely available ANSI C library for computing the Fast Fourier Transform (FFT) in one dimension (1D) with arbitrary grid size. The algorithm is described in the following subsection.

3.1.1 Two-Dimensional Fast Fourier Transform

In the first step, the two dimensional data is partitioned into N smaller blocks, each block contains a subset of rows, as shown in Figure (3.). The size of these blocks is chosen that each block fit in the memory. The 1-D FFTs concurrently can be achieved to each block, by allowing whole CPU to compute an entire 1-D FFT for all rows simultaneously.

H_1
.
.
H_N

Figure 3: Blocked row distributions.

When the row FFTs are complete, the data is remapped so that each row block (HI) is written as block matrices contain a subset of columns, as shown in Figure (4.) and each block is stored in the external memory. N×M buffers are used to store the result of one-dimensional FFTs over the rows.

H_{I1}	……….	H_{IM}

Figure 4: Blocked column distributions.

The second step consist to transpose the data, this step is standard matrix transposition applied on each of blocks. And blocks are arranged as shown in Figure (5.).

H_{11}^T	……….	H_{N1}^T
. . . .	. . . .	. . . .
H_{1M}^T	………..	H_{NM}^T

Figure 5: Matrix transpose.

The transpose rearranges the data so that a second set of 1-D FFTs can be achieved as the first step. A final transpose puts the data back to the correct input order.

3.2 The Beam Propagation Method (Finite Difference Approximation)

This chapter describes how the optical field can be determined by means of finite-difference calculations based on the parabolic wave equation. To obtain the parabolic wave equation, we use the slowly varying envelope approximation [16]. This assumption allows simplification of the second-order partial derivative of U in the propagation z direction and accurate computation at significantly larger steps in the propagation z direction. According to this assumption the optical field U can be written as the product of a factor e^{-jkz}, describing the propagation of a plane wave in free space in the z direction, and a function u, describing the modulations of the wave field [10] [11] [12]. The field is then expressed as [9]:

$$U(x,y,z) = u(x,y,z)e^{-jkz} \tag{12}$$

Ignoring the second-order partial derivative of u in the z direction and substituting Eq. (12) into Eq. (6) yields

$$\frac{\partial^2 u}{\partial x^2} + \frac{\partial^2 u}{\partial y^2} - 2jk\frac{\partial u}{\partial z} + k^2(n^2-1)u = 0 \tag{13}$$

Given an input optical field $u(x,y,0)$, the above equation determines the evolution of the field in the space $z > 0$. For a numerical solution of the parabolic wave equation (13) in the domain Ω (fig 6.), we extend the above model by the use of the following boundary condition on $\partial\Omega = \Sigma \cup \tilde{\Sigma} \cup \Gamma$:

- $U(x,y,0) = U_i(x,y)$, U_i is the given field incident on Σ.
- $\frac{\partial u}{\partial n} = iCu$, ($\frac{\partial}{\partial n}$ denotes the derivation in direction of the outer normal), Robin boundary condition was used on Γ instead of a reflecting boundary condition to reduce the reflection at the absorption gradient.

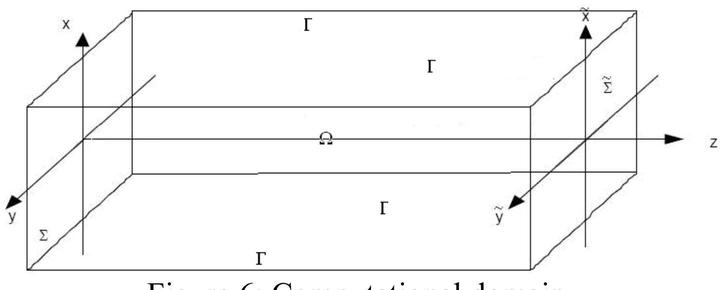

Figure 6: Computational domain.

For convenience we define

$$\alpha = -\frac{j}{2k} \quad ; \; B = -\frac{jk}{2}(n^2 - 1)$$

and the parabolic wave equation take the following form:

$$\frac{\partial u}{\partial z} = \alpha\left(\frac{\partial^2 u}{\partial x^2} + \frac{\partial^2 u}{\partial y^2}\right) + \beta u \tag{14}$$

For a numerical solution of the wave equation (14), we calculate u(x, y, z) on a grid of $N_x + 1$, $N_y + 1$, and $2N_z + 1$ points equidistantly spaced by Δx, Δy and Δz in the respective directions (Fig. 6.). We define

$$u_{ij}^k = u(i\Delta x, j\Delta y, k\Delta z).$$

We use a two-step alternating-direction implicit finite-difference scheme based on the Peaceman–Rachford scheme [13] that is second-order accurate in Δx, Δy and Δz. In each step, the increment in the z direction is $\Delta z / 2$. In the first step, the parabolic wave equation is approximated by the finite difference equation, the partial derivative with respect to x is evaluated implicitly, while the partial derivative with respect to y is evaluated explicitly.

$$\begin{aligned} 2\frac{u_{ij}^{n+0.5} - u_{ij}^{n}}{\Delta z} &= \alpha \frac{u_{(i-1)j}^{n+0.5} - 2u_{ij}^{n+0.5} + u_{(i+1)j}^{n+0.5}}{\partial x^2} + 0.5\beta_{ij}^{n+0.5} u_{ij}^{n+0.5} \\ &\quad + \alpha \frac{u_{(i-1)j}^{n} - 2u_{ij}^{n} - u_{(i+1)j}^{n}}{\partial y^2} + 0.5\beta_{ij}^{n} u_{ij}^{n} \end{aligned} \tag{15}$$

In the second step, we evaluate the partial derivatives with respect to y implicitly and with respect to x explicitly.

$$\begin{aligned} 2\frac{u_{ij}^{n+1} - u_{ij}^{n+0.5}}{\Delta z} &= \alpha \frac{u_{(i-1)j}^{n+1} - 2u_{ij}^{n+1} + u_{(i+1)j}^{n+1}}{\partial y^2} + 0.5\beta_{ij}^{n+1} u_{ij}^{n+1} \\ &\quad + \alpha \frac{u_{(i-1)j}^{n+0.5} - 2u_{ij}^{n+0.5} - u_{(i+1)j}^{n+0.5}}{\partial x^2} + 0.5\beta_{ij}^{n+0.5} u_{ij}^{n+0.5} \end{aligned} \tag{16}$$

We shall use the following notation:

$$\{u\}_i^k = \begin{bmatrix} u_{i1}^k \\ . \\ . \\ u_{iN_y}^k \end{bmatrix} \text{ and } \{u\}_j^k = \begin{bmatrix} u_{1j}^k \\ . \\ . \\ u_{N_x j}^k \end{bmatrix}.$$

Taking into account the boundary conditions, the algorithm can be summarized in matrix notation as follows:

Algorithm:

1. $u_{ij}^{0} = u(i\Delta x, j\Delta y, 0)$, $i = 1,..,N_x$, $\mathrm{j} = 1,..,\mathrm{N_y}$ given.
2. for $n \geq 0$. $u_{ij}^{n} = u(i\Delta x, j\Delta y, n\Delta z)$, $i = 1,..,N_x$, $\mathrm{j} = 1,..,\mathrm{N_y}$ given
   - we solve $\left[A_j\right]\{u\}_j^{n+(1/2)} = \{r\}_j, j = 1,..,N_y - 1$,
   - we solve $\left[B_i\right]\{u\}_i^{n+1} = \{r\}_i, i = 1,..,N_x - 1$.

Where the matrix $\left[A_j\right], \left[B_i\right]$ and vectors $\{r\}_i, \{r\}_j$ are implicitly expressed, depending only on quantities computed previously and can be easily calculated. More details on the algorithm can be found in the reference by Christian Fuhse (2006) [16].
In this algorithm, $\left[A_j\right]$and$\left[B_i\right]$matrix are tridiagonal, the three-diagonal systems of linear equations are solved by standard elimination method and iterative method, described in [14] [16]. For very large computation domain, the FD-BPM method is efficient in terms of computer time and memory than other methods for example finite element method (FEM) or boundary element method (BEM).

4 Results and Conclusion

In order to analyse and estimate the results of the proposed algorithms, we have implemented the algorithms according to the procedure described above in which the recording and reconstruction of a computer-generated hologram can be simulated by means of a computer.

4.1 Numerical Simulations using FFT-BPM algorithm

4.1.1 The first example

The simulated object is the picture of 2560×2560 pixels with pixel distances $\Delta x = \Delta y = 7.4\mu m$ shown in the Table 1(a), the distance between the hologram plane and the object is $d_0 = 1m$. The hologram was designed with the parameter $\lambda = 0.514\mu m$ and $N_x = N_y = 9386$.With these values, the pixel distances in the hologram plane and in the image plane are $\Delta\widetilde{x} = \Delta\widetilde{y} \approx 7.4\mu m$.

The reconstruction results of from the simulated digital hologram and of the reconstructed intensity from hologram obtained by computer simulation are depicted in Table 1. The reconstruction agrees very well with the simulated object at the position of the reel image.

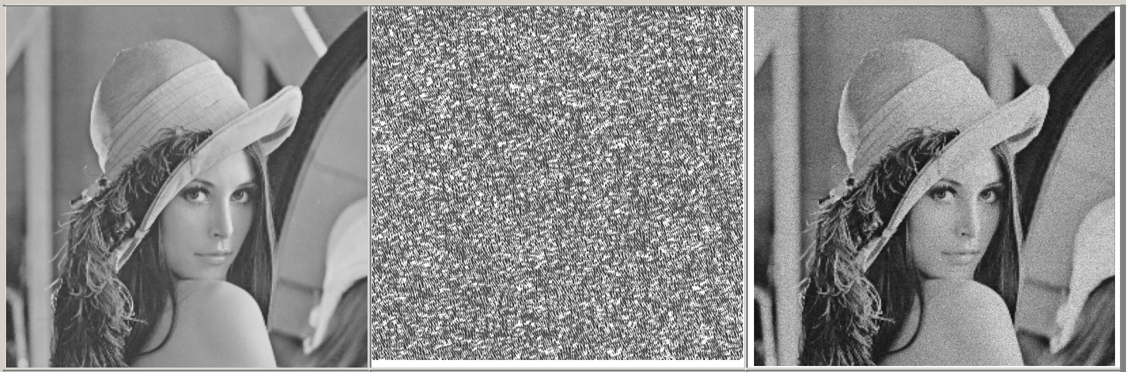

a) Object	b) Simulated digital hologram	c) Reconstructed intensity image

Table1: The object, the simulated digital hologram and the reconstructed intensity image.

4.1.2 The second example

The simulated object is the USAF1951 resolution target of 13700×13700 pixels with pixel distances $\Delta x = \Delta y = 7.4\mu m$ shown in the Table 2(a), the distance between the hologram plane and the object is $d_0 = 1m$. The hologram was designed with the parameter $\lambda = 0.514\mu m$ and $N_x = N_y = 32125$.

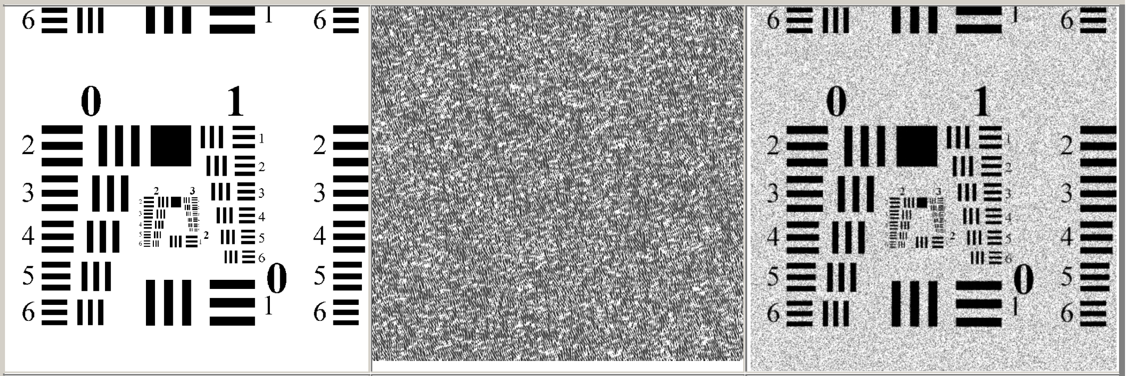

a) Object	b) Simulated digital hologram	c) Reconstructed intensity image

Table2: The object, the simulated digital hologram and the reconstructed intensity image.

The reconstruction results of from the simulated digital hologram and of the reconstructed intensity from hologram obtained by computer simulation are depicted in Table 2. The reconstruction agrees very well with the simulated object at the position of the reel image.

4.2 Numerical Simulations using FD-BPM algorithm

The simulation is limited to a small object only of 256×256 pixels with pixel distances $\Delta x = \Delta y = 2.5\mu m$ shown in the Table 1(a), the distance between the hologram plane and the object is $d_0 = 1cm$. The hologram was designed with the parameter $\lambda = 0.514\mu m$ and $N_x = N_y = 512$. The calculations are carried out with different longitudinal step sizes Δz and of the reconstructed intensity from hologram obtained by computer simulation are depicted in Table 3.

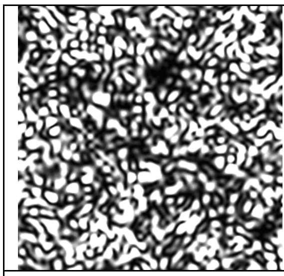	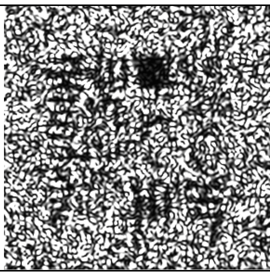	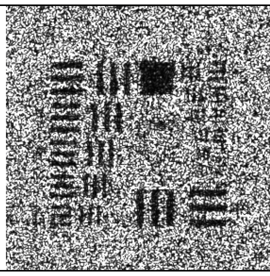	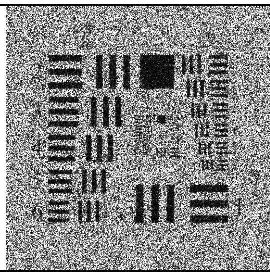
(a) $\Delta z = 1.0\mu m$	(b) $\Delta z = 0.5\mu m$	(c) $\Delta z = 0.25\mu m$	(d) $\Delta z = 0.1\mu m$

Table3: The reconstructed intensity image.

As the large longitudinal step size decreases further, as shown in Table 3, the calculated results become accurate and it is accompagnied by the increase of the total computation time. This method is extremely accurate for small object and small reconstruction distance and may be used in digital holographic microscopy. At large reconstruction distance and large object, its accuracy deteriorates rapidly, this behavior results from the accumulated numerical error. The main disadvantage of this method is that it consists of solving $N_x + N_y - 2$ independent systems of linear equations at each step, which makes it slow. It is possible to parallelize this part of the algorithm. Furthermore, the computation time reduction can be achieved if the computational domain is truncated by using an artificial boundary such a perfectly matched layer (PML).

4.3 Conclusion

In this paper, two methods for generating and reconstructing digital hologram are described. Both of these methods were tested numerically using one processor machine and the results of the test are presented and show acceptable agreement between the simulated object and the reconstructed intensity image. The first method based on FFT-BPM algorithm is recommended for very large reconstruction distance and large object while the second FD-BPM is recommended for small object and small reconstruction distance.

The aim of future work is essentially to parallelize the code to improve performance of these algorithms and to introduce a perfectly matched layer boundary condition to truncate the computational domain for the second method

References

[1] J.W. Goodman: Introduction to Fourier Optics, 2nd edition. McGraw-Hill Companies, Inc., New York, 1996.

[2] Kronrod R.W., Merzlyakov N.S., Yaroslavskii L.P.: Reconstruction of a hologram with a computer. Sov. J. Tech. Phys. 1972. V.17. P. 333–334.

[3] Schnars U.: Direct phase determination in hologram interferometry with use of digitally recorded holograms. J. Opt. Soc. Am. A. 1994. V.11. P. 2011-2015.

[4] Schanrs U, Jüptner W.: Direct recording of holograms by a CCD target and numerical reconstruction. Appl. Opt. 1994. V.33. P. 179-181.

[5] Schnars U., Jüptner W.: Digital recording and numerical reconstruction of holograms. Meas. Sci. Technol. 2002.V.13. P. R85–R101.

[6] Pan G.: Meng H. Digital holography of particle fields: reconstruction by use of complex amplitude. Appl. Opt. 2003. V.42. P. 827-833.

[7] M. Born and E.Wolf: Principle of Optics, 7th (expanded) edition. Cambridge University Press, 1999.

[8] Goodman J.W., Lawrence R.W. Digital image formation from electronically detected holograms. Appl. Phys. Lett. 1967. V.11. P. 77–79.

[9] A.C. Kak and M. Slaney: Principles of Computerized Tomography. IEEE Press, 1983.

[10] Yee, K.: Numerical solution of initial boundary value problems involving Maxwell´s equations in isotropic media, IEEE Transactions on Antennas and Propagation, 14, 1966, pp. 302-307.

[11] Zhou, P.: Numerical Analysis of Electromagnetic Fields. Springer, Berlin Heidelberg, 1993.

[12] G. Mur: Absorbing boundary conditions for finite difference approximation of the time-domain electromagnetic field equations, IEEE Trans. Electromagn. Compat. 23, 377–382 (1981).

[13] J. W. Thomas: Numerical Partial Differential Equations (Springer-Verlag, 1995).

[14] B. Mohammadi, J.H.Saiac: Pratique de la simulation numérique ; Dunod, 2003.

[15] A. Lotfi: Computer Generated Hologram, ICNAAM, Proc. Int. Conf. on Numerical Analysis and Applied Mathematics, Creta, 2006 szept, 203-207.

[16] C. Fuhse: X-ray waveguides and waveguide-based lensless imaging. PhD thesis, University of Göttingen, (2006).